

# The Proper Motion and Parallax of Barnard's Star: Errors and Precision in Small-Telescope Astrometry

Richard Berry  
Alpaca Meadows Observatory  
22614 N Santiam Hwy  
Lyons, OR 97358  
rberry@wvi.com

---

## Abstract

This paper examines a series of measurements made to determine the proper motion and parallax of Barnard's Star using differential astrometry. In differential astrometry, the same reference stars are used for every coordinate determination. Although the absolute coordinate solution is offset by a constant due to the imprecisely known positions of the reference stars, relative coordinate solutions can be precise. For this study, observations of the field of Barnard's Star were made in 2009 and 2010 using an 8-inch  $f/4$  Newtonian telescope. The single-night standard error in each coordinate can be as low as 10 mas. We discuss the errors, error distribution, and error sources in the astrometric solution, as well as the derived proper and parallax motions of the star.

---

## 1. Introduction

This study began as a project for students attending the 2009 Pine Mountain Observatory Summer Research Workshop. The goal was to answer the question: Is it possible to detect the proper motion of Barnard's Star over the course of the three-night workshop? Intrigued by the question, I can now answer that it is possible to do so in a *single* night using a small-aperture short-focus telescope with a CCD camera. This paper describes what I learned about factors that affect small-telescope astrometry, and analyzes image data taken in 2009 and 2010.

## 2. Small-Telescope CCD Astrometry

Astrometry is the science of measuring the positions and motions of celestial objects. To measure the right ascension and declination of an object such as Barnard's Star, the observer takes CCD images of the object. Each image is associated with the time it is taken. Each image must show the object in question plus at least three reference stars, that is, stars whose celestial coordinates,  $(\alpha, \delta)$ , are known accurately.

The observer measures the image to obtain an  $(x, y)$  position for each of the reference stars and the target object. Then  $(X, Y)$  standard coordinates (i.e., coordinates on a plane tangent to the celestial sphere at the center of the image), are computed for each reference star from its celestial coordinates. Then a least-squares fit to a general linear transform between the  $(x, y)$  and  $(X, Y)$  coordinates is determined, such that for every  $(x, y)$  it is possible to find the corre-

sponding  $(X, Y)$ . To derive the position of the target object, the measured  $(x, y)$  coordinates of the target object are converted into  $(X, Y)$  standard coordinates, and then into  $(\alpha, \delta)$  for the target object (Berry *et al.*, 2005a).

It is possible, with only modest attention to technique, to measure the  $(\alpha, \delta)$  coordinates of a star, asteroid, or comet with an accuracy and precision better than 1 arcsecond. Measuring the proper motion and parallax of a star requires precision but not accuracy, and requires attention to factors that may introduce very small random and systematic errors. Measuring Barnard's Star enabled me to explore the errors and sources of errors amounting to a small fraction of 1 arcsecond.

## 3. Observations

The Barnard's Star dataset consists of 836 images taken on 20 nights; 11 nights in 2009 and 9 nights in 2010. On 18 nights, the images were obtained using an 8-inch  $f/4$  Vixen R200SS reflecting telescope, a TeleVue ParaCorr coma correcting lens, and a Quantum Scientific QSI 532ws CCD camera using Schuler BVRI and clear filters, from Alpaca Meadows Observatory ( $-122.6^\circ$ ,  $+44.8^\circ$ ) in Oregon. Images on the other two nights were taken at the Pine Mountain Observatory ( $-120.9^\circ$ ,  $+43.8^\circ$ ) in Oregon with a Celestron 11-inch EdgeHD SCT using the same camera and filters.

Table 1 is a journal of observations listing, for each night, the number of useable images, the telescope, filters, and exposures used.

Date	Optics	Filter	Exp (s)	N
2009-06-27	R200SS	BVRI	60	14
2009-07-16	11" EHD	BVRI	20	47
2009-07-17	11" EHD	BVRI	60, 20	40
2009-07-24	R200SS	V	10, 20, 50	27
2009-08-16	R200SS	V	50	20
2009-08-23	R200SS	VR	30	40
2009-09-10	R200SS	V	20	40
2009-09-25	R200SS	V	20	20
2009-10-06	R200SS	V	20	20
2009-11-01	R200SS	V	20	92
2009-11-24	R200SS	V	20, 30	40
2010-02-20	R200SS	V	20, 40	40
2010-06-07	R200SS	V	20, 40	36
2010-07-03	R200SS	V	60	32
2010-07-05	R200SS	V	60	59
2010-08-15	R200SS	V	60	58
2010-09-12	R200SS	V	60	58
2010-09-24	R200SS	V	60	58
2010-09-25	R200SS	V	60	59
2010-10-19	R200SS	V	60	57

**Table 1: Journal of observations of images of the field of Barnard's Star made on 20 nights during 2009 and 2010.**

In the early image sets taken with more than one filter, the filters were interleaved to minimize changes in non-filter properties such as focus drift. In image sets with multiple exposure times, different exposures were interleaved, again to minimize differences not caused by factors other than exposure.

Observations made during 2009 served primarily to test techniques and explore sources of error as I experimented with different filters and exposure times. In 2010, I applied the lessons learned, standardizing on 60 image sets of 60-second exposures made with a V filter.

Images made to determine proper motion can be taken at any time of the year, but for determination of parallax, it is desirable to capture images when the star in question is near the ends of its parallactic ellipse. Since Barnard's Star attains solar conjunction on December 20, it stands near extremes of its ellipse in late March and late September. Oregon weather strongly favors summer and fall observation, so the dataset contains no images from March, April, or May. However, June through October is well-represented, and I did obtain just-after-sunset images in November 2009 and just-before-sunrise images in February 2010.

#### 4. Image Reduction

Reduction from images to nightly mean positions of Barnard's Star was carried out using *AIP4Win* and *Microsoft Excel 2003*<sup>®</sup>. In June 2009, I made test exposures of the field around Barnard's Star to select a group of eleven reference stars, and at the PMO Summer Research Workshop, obtained large-scale

images. Figure 1 shows the reference stars, and they are listed in Table 2. The selection criteria were that the star be single, separate from faint companions, and sufficiently close to Barnard's Star to fall inside the center half of the field in the 11-inch EdgeHD telescope. This means that the reference stars occupy a small portion of the field of the Vixen R200SS.

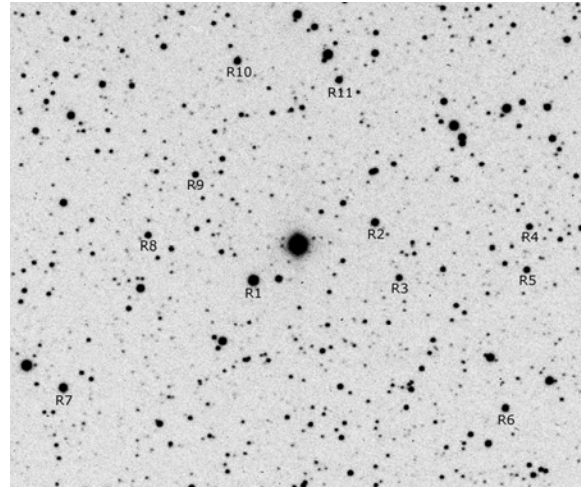


**Figure 1: The starfield around Barnard's Star. The reference stars used in this study are labeled R1 through R11. Table 2 shows data for the reference stars.**

Star	$\alpha$	$\delta$	$M_{\text{cat}}$	B-V
R1	17 57 51.96	+04 42 20.2	11.45	-0.1
R2	17 57 40.88	+04 43 53.9	13.03	+0.8
R3	17 57 38.21	+04 42 39.0	14.15	+0.5
R4	17 57 26.27	+04 44 03.9	14.25	+0.2
R5	17 57 26.21	+04 43 03.8	14.08	+1.0
R6	17 57 27.24	+04 39 45.9	13.72	+0.8
R7	17 58 09.13	+04 39 27.6	12.65	-0.0
R8	17 58 09.13	+04 43 11.7	14.05	+0.8
R9	17 57 58.16	+04 44 42.1	14.37	+0.3
R10	17 57 55.01	+04 47 27.6	13.55	+0.7
R11	17 57 45.28	+04 47 11.6	13.58	+0.8

**Table 2: Reference stars used in this study. Coordinates and catalog magnitudes ( $M_{\text{cat}}$ ) are from UCAC2. B-V colors based on instrumental magnitudes, adjusted to match Tycho data for R1 (TYC 425-262).**

For reduction, I used the astrometry function in the Magnitude Measurement Tool in *AIP4Win* (Berry, 2005b). To perform astrometry on a set of images, a set of reference stars are selected on a master image, then each image in the set is automatically dark subtracted and flat-fielded, the stars are measured, a plate solution computed, and the coordinates of the target stars with auxiliary data are written to a text-format file. Sample output showing the first ten images in a 60-image set is given in Table 3. Key results are the JD of the image, the RA and Dec in decimal degrees, and the residuals of the plate solution in seconds of arc. Diagnostics include the derived focal length of the telescope, the position angle

Table 3: Sample Raw Astrometric Output											
Seq#	JulianDay	Focal	PA[d.d]	X[pix]	Y[pix]	RA[d.d]	Dec[d.d]	RArms	DCrms	HMMSS.ss	+DDMMSS.s
0000	2455465.471898	911.0738	174.8909	1109.115	724.255	269.449540	4.724217	0.145	0.092	175747.89	+044327.2
0001	2455465.472859	911.1903	174.9034	1110.339	725.270	269.449559	4.724245	0.137	0.086	175747.89	+044327.3
0002	2455465.473831	911.0766	174.8860	1110.757	725.883	269.449519	4.724284	0.118	0.048	175747.88	+044327.4
0003	2455465.474803	911.1803	174.8925	1111.659	726.666	269.449526	4.724268	0.160	0.072	175747.89	+044327.4
0004	2455465.475775	911.2407	174.8792	1112.475	726.338	269.449534	4.724249	0.101	0.083	175747.89	+044327.3
0005	2455465.476736	910.8706	174.8941	1113.099	726.950	269.449537	4.724278	0.149	0.112	175747.89	+044327.4
0006	2455465.477708	910.8468	174.8869	1113.264	726.589	269.449533	4.724270	0.144	0.086	175747.89	+044327.4
0007	2455465.478669	910.9625	174.8899	1114.228	726.405	269.449547	4.724234	0.108	0.100	175747.89	+044327.2
0008	2455465.479641	920.5098	173.9535	1114.788	726.566	269.449874	4.724502	4.913	3.134	175747.97	+044328.2
0009	2455465.480602	911.0141	174.8864	1115.220	726.386	269.449559	4.724228	0.077	0.081	175747.89	+044327.2

**Table 3: Raw astrometric output includes the sequence number of the image, the JD, the focal length of telescope and position angle of the +x axis of the image derived astrometrically, the (x,y) coordinates of the star, the ( $\alpha,\delta$ ) coordinates of the star in decimal degrees, the RA and Dec residuals of the astrometric fit, and the ( $\alpha,\delta$ ) in sexigesimal format.**

of the +x axis of the image, and the (x,y) coordinates of the target star.

The text file is imported into Excel for analysis. For each night’s data, the following are computed:

- mean JD;
- the mean, standard deviation, and standard error of the RA determination;
- the mean, standard deviation, and standard error of the Dec determination;
- the mean and standard deviation of the residual in RA; and
- the mean and standard deviation of the residual in Dec.

If the measured (x,y) coordinates of the reference stars on an image matched exactly the computed (X,Y) coordinates, the residual of the astrometric solution would be zero. But the combination of reference star position uncertainties in the astrometric catalog and random errors in the reference star centroids measured from the images produce non-zero residuals. The positions are, therefore, positions relative to the specific set of reference stars.

Other factors that potentially affect the solution include distortion and color errors in the optical system, tracking errors, focus errors, filter-related color effects, and the displacement of the star by atmospheric refraction. These are discussed in § 5 below.

In a sequence of images, the expectation is that catalog errors contribute a constant residual because these are errors are the same for every image, while the centroid errors contribute random variations. This behavior is, in fact, seen in the data. For the night shown in the example, 2010-09-25, the mean residual in RA is  $141 \pm 27$  mas, and in declination,  $90 \pm 24$  mas (mas = milli-arcseconds). As a cross-check, the standard deviation in the computed RA coordinate is 77 mas, and in the Dec coordinate, 71 mas. The anticipated and measured errors are thus reasonably consistent with one another.

On occasion, however, outlying values are seen. For image Seq# 0008, the residuals in RA and Dec are 4.9 and 3.1 arcseconds, and the solutions for the focal length and position angle lie well outside the normal range. Although the reason was not evident from inspection of this particular image, I rejected this line of data. In many cases, however, the large residuals have obvious causes: a “blow-up” in the seeing, severe image trailing, a cosmic ray near one of the reference stars, or the loss of one of the fainter stars due to a cloud or a passing airplane contrail. Among the images made in 2010, 2.6% of coordinate measurements were rejected as outliers.

After removing outliers, the mean of the RA and Dec coordinates is taken as the nightly position, and the standard error (*i.e.*, the standard deviation divided by the square root of the number of images) is the error associated with that position. For the remaining 59 images in the example, the standard error is 10.1 mas in RA and 9.2 mas in Dec.

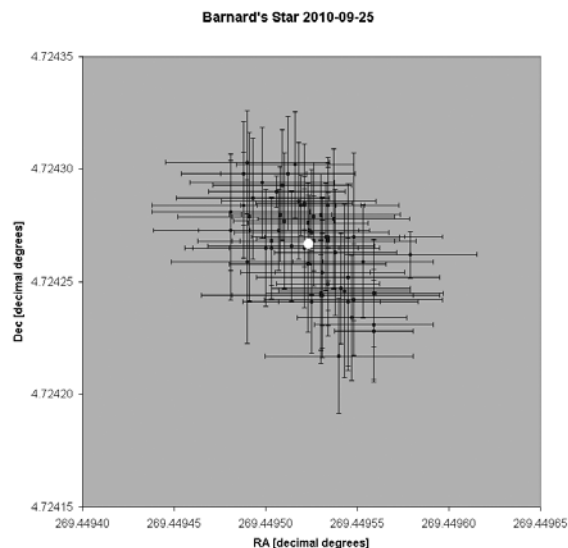


**Figure 2: This plot shows the positions and error bars determined for Barnard’s Star from 59 individual images made on 2010-09-25. The large white dot is the mean value. The plot area is 0.9 arcseconds square.**

Table 4: Mean positions and standard errors of Barnard's Star for 20 Nights in 2009-2010						
Date	JD	RA	Dec	RA <sub>ste</sub>	Dec <sub>ste</sub>	N
2009-06-27	2455010.81407	269.44994707	4.72076871	0.00000388	0.00000576	14.00
2009-07-16	2455028.80895	269.44987810	4.72090612	0.00000165	0.00000165	41.00
2009-07-17	2455030.80288	269.44989435	4.72092106	0.00000354	0.00000189	31.00
2009-07-24	2455037.76499	269.44984252	4.72096489	0.00000846	0.00000717	27.00
2009-08-16	2455060.70775	269.44980920	4.72112190	0.00000819	0.00000548	20.00
2009-08-23	2455067.71629	269.44978710	4.72116720	0.00000521	0.00000493	40.00
2009-09-10	2455085.65938	269.44975914	4.72129771	0.00000478	0.00000506	35.00
2009-09-25	2455100.68891	269.44975095	4.72138550	0.00000908	0.00000780	20.00
2009-10-06	2455111.61915	269.44973775	4.72147455	0.00000709	0.00000671	20.00
2009-11-01	2455137.60667	269.44975657	4.72163799	0.00000473	0.00000389	92.00
2009-11-24	2455160.57452	269.44977870	4.72180378	0.00000514	0.00000480	40.00
2010-02-20	2455249.06188	269.44995185	4.72252358	0.00000398	0.00000548	40.00
2010-06-07	2455355.80518	269.44978542	4.72349878	0.00000340	0.00000284	36.00
2010-07-03	2455381.78179	269.44969725	4.72369041	0.00000509	0.00000338	32.00
2010-07-05	2455383.75921	269.44969846	4.72370029	0.00000373	0.00000283	59.00
2010-08-15	2455424.72041	269.44958083	4.72399322	0.00000255	0.00000224	58.00
2010-09-12	2455452.55843	269.44952409	4.72418109	0.00000331	0.00000235	58.00
2010-09-24	2455464.52788	269.44952317	4.72426181	0.00000293	0.00000242	58.00
2010-09-25	2455465.50082	269.44952351	4.72426698	0.00000279	0.00000255	59.00
2010-10-19	2455489.64844	269.44952582	4.72441151	0.00000261	0.00000335	57.00

Table 4: Mean positions and standard errors of Barnard's Star measured in 2009 and 2010.

Figure 2 shows a plot of the position of Barnard's Star in each of the 59 accepted images. The error bars show the standard deviation of each of the individual measurements. The large white point in the center is the mean position. The plot area is 0.9 arcseconds square.

Table 4 summarizes the positions and standard errors determined on the 20 nights in 2009 and 2010 from which the proper motion and parallax were computed. Positions are given in decimal degrees. To put the standard errors into context, 1 arcsecond is  $0.000277^\circ$ , while the mean standard error in RA for the entire dataset is  $0.0000046^\circ$ , or 16.5 mas. The mean standard error is 14.9 mas in declination, and their sum is 22.2 mas. This angle corresponds to 97 nanometers in the focal plane of the telescope.

From inspection of Table 4, it is clear that after I established a consistent procedure for imaging (60 images of 60 seconds exposure with a V filter), there was a significant improvement in the quality of the results.

## 5. Sources of Error

Ordinarily astrometry relies on several basic assumptions, namely: 1) that the optical system maps the sky onto the focal plane as  $r = F \cdot \tan(\theta)$ , where  $r$  is the radial distance,  $F$  is the focal length, and  $\theta$  is the angular distance from the optical axis of the telescope, 2) that star images are symmetrical and identical over the field of view, and 3) that the atmosphere has a negligible effect on the location of star images. At the scale of a few arcseconds and the linear dimensions of a pixel, these are reasonable assumptions. At sub-arcsecond and sub-pixel scales, they break down.

## 5.1 Optics

Newtonian telescopes suffer from coma, an aberration which produces asymmetric star images that become increasingly asymmetric with increasing off-axis distance. To correct coma, I made my images with an auxiliary TeleVue ParaCorr lens. It is likely that this optic introduces small departures from  $F \cdot \tan(\theta)$  mapping. Furthermore, it may introduce small amounts of lateral chromatic aberration, causing the radial distance from the optical axis to vary with wavelength. This effect would displace red stars relative to bluer stars, and affect the astrometric solution.

To minimize these effects, I consistently placed Barnard's Star close to the center of the image and chose reference stars close to Barnard's Star and at approximately the same radial distance. With the images available, I was not able to test for distortion or lateral chromatic effects.

## 5.2 Reference Stars

The parallax and proper motion of a nearby star is measured against the backdrop of more distant reference stars, but these too have proper motions, and their catalog positions have uncertainties. The values derived directly are relative to these background stars. Only when the proper motions and parallaxes are known with sufficient accuracy is it possible to solve for the absolute parallax and proper motion.

The reference stars listed in Table 2 are all considerably bluer than Barnard's Star, an M5 dwarf. This poses problems for astrometry of Barnard's Star, since any color-sensitive effects in the optics or atmosphere can displace Barnard's Star relative to the suite of reference stars. Barnard's Star has a B-V

color of +1.3, while the reference stars vary from  $B-V \cong -0.1$  to +1.0. Any color sensitive displacements will affect the astrometric solution.

Bennett (2007) provides a list of reference stars with relative proper motions from Leander McCormick and the Tycho catalog. Using these as reference stars instead of those I did use and reducing the images again might be worth while. On the other hand, the stars I used are much fainter than the McCormick stars, and are thus on the average more distant and have smaller proper motions.

### 5.3 Telescope Side of the Pier

Telescopes on German equatorials must be “flipped” to observe objects east or west of the meridian. Doing so introduces instrument flexure. In the Vixen R200SS, flexure occurs in the tube supporting the focuser. The net effect is a change in the collimation of the optics and small tilt in the coma corrector.

To check for east *versus* west errors, I compared the difference between the model ellipse and the observed position against the position angle of north, and did not see an obvious correlation between them.

### 5.4 Image Trailing

Most of the images taken in 2009 were made without a guide telescope. Those taken in 2010 were made using a guide telescope and autoguider. In both cases, the stars in many images are not perfectly round, and in some cases, they are markedly trailed.

I compared the residuals from images with round or nearly round stars against those with trailed and markedly trailed star images, and did not see an obvious correlation. It appears that centroid determination is as repeatable for identical but non-round images as it is for round images.

### 5.5 Image Calibration

During reduction using AIP4Win’s MMT Astrometry function, images are routinely dark-frame subtracted and flat-fielded. However, the CCD in the camera is fairly “clean” of hot pixels. As a test, I ran the same group of images with and without dark and flat calibration.

Plotting calibrated against non-calibrated RA and Dec coordinates showed a one-to-one correspondence and a total spread of  $\sim 36$  mas in each coordinate. Plotting the residuals in RA and Dec also showed a one-to-one correspondence. Barring the odd instance when a reference star might fall directly on a high-

value hot pixel, calibration did not appear to affect the astrometric measurements.

### 5.6 Atmospheric Refraction and Dispersion

Atmospheric dispersion is known to have the potential to introduce major errors, especially when the color of the target star differs from that of the reference stars. On four nights in 2009, I made image sets through BVRI or VR filters to assess the magnitude of this source of errors.

Figure 3 plots the position of Barnard’s Star determined from 20 V-filtered images compared to 20 R-filtered images taken on 2009-08-23. The V-filtered position is 132 mas north of the R-filtered position, far in excess of the standard error of  $\sim 30$  mas. Note that this displacement, at the scale of my images, is about one-tenth of a pixel.

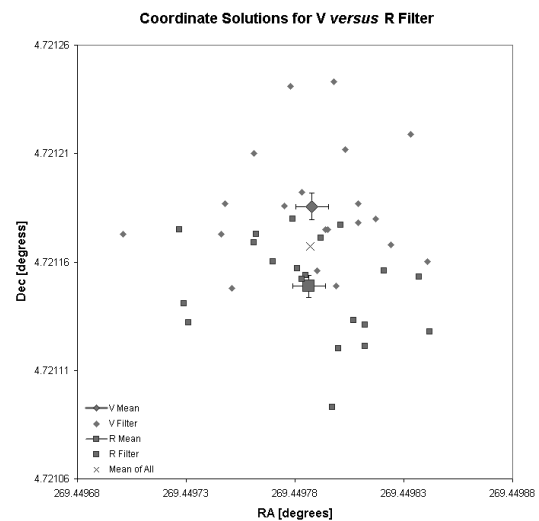


**Figure 3: Atmospheric dispersion is a significant effect. In this graph showing coordinates derived from 20 images made with a V filter and 20 images made with an R filter, the separation between the mean positions is 132 mas. Error bars show the standard error for the mean V and R positions.**

The displacement of Barnard’s Star occurs because the effective wavelength of its image differs from that of the much bluer reference stars (van de Kamp, 1967). A similar but smaller displacement occurs within a single filter band; that is, the effect within a V-filter image is smaller than the difference between the V-filter images and R-filter images.

During the 2010 observing season, images were taken with a V filter only and close to the meridian whenever it was practical. Although atmospheric dispersion is smaller at R-filter wavelengths, I chose the V filter to reduce the brightness of Barnard’s Star relative to the reference stars.

During the 2009 and 2010 observing seasons, Barnard's Star did not always reach the meridian before morning twilight began, or it had already passed the meridian before evening twilight ended, so I imaged the field away from the meridian, at lower elevation angles above the horizon.

Looking ahead, Figure 6 shows the observations and the model parallactic ellipse together. As expected, the images made in November 2009 and February 2010 show considerably larger deviations from the model ellipse than do images made in August and September. To lessen this effect, images should be taken as close to the meridian as practical. Although the image of a very red star will still be displaced at the meridian, the displacement will be constant.

### 5.7 Number of Images

To reduce the standard error, during the 2010 observing season I increased the number of images taken each night to 60. I also increased the exposure times to 60 seconds to provide better photon statistics for the centroiding algorithm. It is possible and practical to make sixty 60-second exposures and keep them at least approximately centered on the meridian. Because the standard error is divided by the square root of the number of images, further increasing the number of images will likely run into the law of diminishing returns.

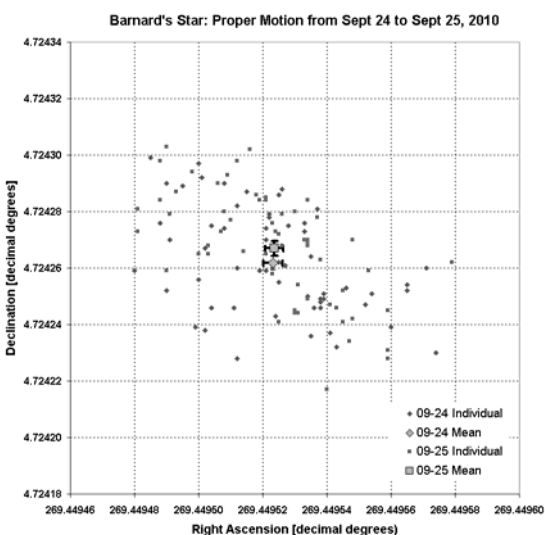


Figure 4: By combining a large number of coordinate determinations, in this case from 59 images, it is possible to “beat down” random noise sufficiently far to detect the proper motion of Barnard's Star from one night to the next.

Increasing the number of images (and driving down the standard error) turned out to be essential in detecting the proper motion of Barnard's Star from

one night to the next. Figure 4 shows the individual observations and their means for the nights of 2010-09-24 and 2010-09-25. The individual observations form two overlapping clouds slightly displaced from one another. The mean coordinates reveal the proper motion of Barnard's Star during a 24-hour time span.

## 6. Proper Motion and Parallax

Because the proper motion and parallax of Barnard's Star are already well known (Gatewood, 1973; Benedict, 1999; Bartlett, 2007), rather than attempting to determine these values from scratch, my goal was to determine instead how well this study's observed positions correspond to the accepted values for Barnard's Star.

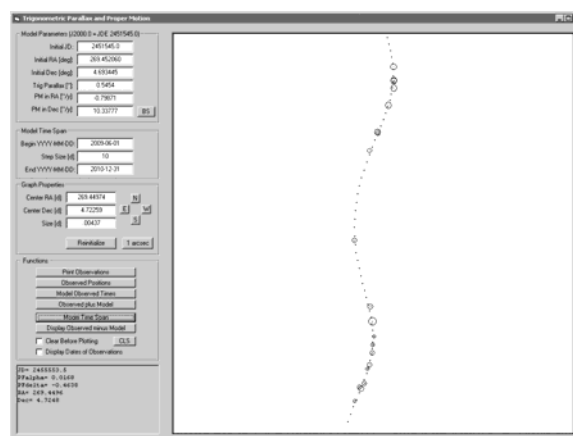


Figure 5: The user interface of TrigParallax shows the observed and model positions for Barnard's Star. The field of view is 0.00437°, or 15.7 arcseconds. Error bars, although they are present, appear too small to see in this plot.

To carry out the comparison, I wrote a computer program (Berry, 2011) to read the observed positions, model the expected positions, and plot results at any scale desired. Figure 5 shows the user interface displaying the observed positions listed in Table 4 in the picture box on the right side. The user enters the model parameters at top left, sets the graphic display properties in the middle, and launches different functions with the buttons near the left side bottom.

The program computes the coordinates of a star,  $(\alpha_t, \delta_t)$ , at time,  $t$ , from the following equations:

$$\alpha_t = \alpha_0 + \mu_\alpha(t - t_0) + \pi P_\alpha$$

$$\delta_t = \delta_0 + \mu_\delta(t - t_0) + \pi P_\delta$$

In these equations,  $(\alpha_0, \delta_0)$  are the heliocentric coordinates of the star at time  $t_0$ , (usually chosen to be J2000.0),  $\mu_\alpha$  and  $\mu_\delta$  are the right ascension and declination components of the star's proper motion,  $\pi$

is the parallax of the star, and  $P_\alpha$  and  $P_\delta$  are the parallax factors in right ascension and declination.  $P_\alpha$  and  $P_\delta$  are functions of the star's position on the celestial sphere relative to that of the Sun, and of the radius vector of the Earth's orbit (van de Kamp, 1967).

Over the course of a year, a star near enough to show parallax describes an ellipse on the sky relative to presumably much more distant reference stars, while also showing proper motion in both right ascension and declination. Default values adopted for the model are:  $\pi = 545.4 \pm 0.2$  mas (Benedict, 1999),  $\mu_\alpha = -798.7 \pm 0.2$  mas/yr, and  $\mu_\delta = 10337.7 \pm 0.2$  mas/yr (Bennett, 2007).

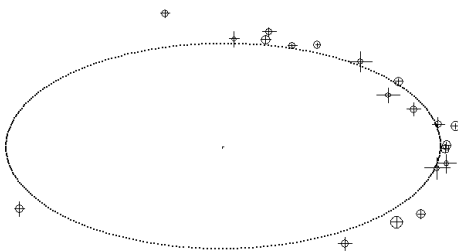


Figure 6: The circles represent observed positions for Barnard's Star, and the small dots show positions computed from the model. The area of the circles is proportional to the number of observations in the point, and the error bars show its standard errors. The major axis of the ellipse is 1.09 arcseconds in length.

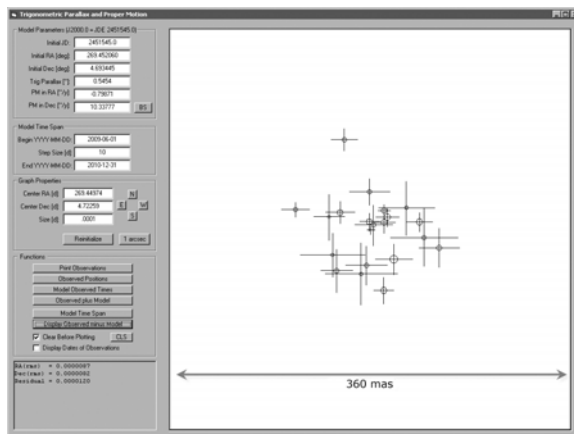


Figure 7: This graph shows the difference between observed positions of Barnard's Star and positions based on the model. Although individual nights show standard errors as low as 10 mas, the r.m.s. error for the entire 2009 to 2010 observing season is 43 mas.

By manipulating the model parameters, the user can remove the proper motion of the star to compare

the observed parallactic ellipse to the computed model, as shown in Figure 6.

The user can also display observed positions minus computed positions (*i.e.*, O-C), showing the errors graphically as in Figure 7. The O-C function also computes the r.m.s. difference between the observed and model positions, which for all 20 nights is 43 mas. The disparity between the mean standard error in all nightly positions (22 mas) and the model fit (43 mas) suggests the presence of long-term systematic errors in the observed positions, as discussed in § 5.

### 7. Further Work

I plan to continue this study for two more years to investigate potential sources of error displacement from atmospheric refraction, from distortion in the optical system, and reference star selection. It is interesting that the single-night precision possible with a small telescope with a CCD camera is comparable to the single-night precision in the classic era of large refractor astronomy (van de Kamp, 1967).

### 8. Conclusion

This study demonstrates that, using differential astrometry, it is feasible to measure relative coordinates of a star to a  $1\sigma$  precision of 10 mas using a small telescope (8-inch  $f/4$  Newtonian) in one hour of data collection. Using the same reference stars for all astrometric solutions minimizes the effects of astrometric catalog errors. However, it is essential to minimize atmospheric dispersion more carefully than I did in this study to attain this precision consistently over the course of a year. The overall precision attained, estimated by comparing the present observations with a model of the proper motion and parallax of Barnard's Star, is on the order of 43 mas.

### 9. References

Bartlett, J. L. (2007) Knowing Our Neighbors: Fundamental Properties of Nearby Stars, Doctoral dissertation, Department of Astronomy, University of Virginia.

Benedict, G. F. *et al.* (1999) Interferometric Astrometry of Proxima Centauri and Barnard's Star Using Hubble Space Telescope Fine Guidance Sensor 3: Detection Limits for Substellar Companions. *Astron. J.* **118**, 1086.

Berry, R., Burnell, J. (2005a) *The Handbook of Astronomical Image Processing*, 2nd Edition, Willmann-Bell, Richmond, VA.

Berry, R., Burnell, J. (2005b) *Astronomical Image Processing for Windows (AIP4Win)*, versions 2.3.34 and 2.4.1, Willmann-Bell, Richmond, VA.

Berry, R. (2011) *TrigParallax*, a computer program, available on request.

Gatewood, G. (1973) An Unsuccessful Search for a Planetary Companion of Barnard's Star (BD+4°3561). *Astron. J.* **78**, 769.

Van de Kamp, P. (1967) *Principles of Astrometry*, W.H. Freeman, San Francisco.